Green Chemistry

Accepted Manuscript

This article can be cited before page numbers have been issued, to do this please use: E. Bartzoka, H. Lange, P. Mosesso and C. Crestini, *Green Chem.*, 2017, DOI: 10.1039/C7GC02009K.

ROYAL SOCIETY OF CHEMISTRY

rsc.li/green-chem

View Article Online
DOI: 10.1039/C7GC02009K

Synthesis of nano and microstructures from proanthocyanidins, tannic acid and epigallocatechin-3-*o*-gallate for active delivery

Elisavet D. Bartzoka,[a] Heiko Lange[a], Pasquale Mosesso,[b] Claudia Crestini[a,]*

a: University of Rome 'Tor Vergata', Department of Chemical Sciences and Technologies, Via della Ricerca Scientifica, 1, 00133 Rome, Italy.

b: University of Tuscia, Department of Ecological and Biological Sciences, Via S. Camillo de Lellis, 44, 01100 Viterbo, Italy.

Corresponding author: **crestini@stc.uniroma2.it*

View Article Online
DOI: 10.1039/C7GC02009K

ABSTRACT

Microcapsules (MCs) and nanoemulsions (NEs) were generated from both condensed and hydrolysable tannins, respectively, for a controllable, stimuli-responsive active release. A rapid, simple and robust one step method based solely on the use of tannins, *i.e.*, without the use of any additional cross-linking reagent, was developed *via* an ultrasound treatment. Condensed tannins *Schinopsis balansae* wood extract (***Sb***) and *Acacia mearnsii* bark extract (***Am***) were studied for their potential to assemble microcapsules, and the hydrolysable tannins tannic acid (**TA**) and epigallocatechin-3-*O*-gallate (**EGCG**) for their potential to form nanoemulsions upon ultrasonic irradiation. Tannin microcapsules (TMCs) and tannin nanoemulsions (TNEs) were thoroughly characterized *via* cryo-SEM, as well as fluorescence and optical microscopy to reveal structural and morphological characteristics. GPC analyses revealed that microcapsules and nanoemulsions were formed due to efficient electronic interactions between the aromatic moieties present in the polyphenolic backbone of high molecular weight fractions of tannins and apparently without any significant chemical modification. Both TMCs and TNEs were formed in high yields and their release efficiencies showed higher stability of the microcapsules compared to nanoemulsions. Active release and pH stability of both the TMCs and TNEs were evaluated. Tannins - and more specifically the polymeric structures of tannins - proofed to be ideal scaffolds for ultrasound assisted capsule assembly with potential in the pH triggered delivery of hydrophobic active molecules.

View Article Online
DOI: 10.1039/C7GC02009K

INTRODUCTION

The benefits of microencapsulation are well established by the extensive research that has been pursued in the recent years worldwide regarding the development of microstructures for the delivery of active substances.[1] The materials employed in the generation of microstructures are of fundamental importance and highly related to the features of the systems to be obtained, hence to their eventual field of application. A variety of types of microstructures has been developed that can be used as vehicles for active delivery, among them polymeric microparticles, liposomes, dendrimers, solid lipid carriers, polymeric micelles, microcapsules (MCs) and nanoemulsions (NEs).[2]

NEs comprise a well perceived delivery system and refer to emulsions with droplet sizes below 1 μm. They are used as carriers for lipophilic drugs prone to hydrolysis. They can be applied as a controlled release delivery system, since they exhibit excellent drug release profiles, due to their very large interfacial area.[3] Another benefit of the reported systems is their stability against sedimentation because of the submicron size of the droplets, as the sedimentation rate due to gravity is less than diffusion and Brownian motion.[4] The tiny droplet size also ensures adequate dose distribution and a good dispersion system. Furthermore, the small size provides large surface areas that ease the solubilisation and penetration capability in *in vivo* administration.[5]A drawback, however, can be the destabilization by Ostwald ripening.[6]

MCs comprise another well studied delivery microsystem and can be easily produced from a NE template.[3] They are endowed with superior characteristics compared to the NEs, such as uniformity and active delivery kinetics. Polymeric MCs can be produced from a NE by '*in situ*' polymerization that is induced from the high energy emulsion polymerization method chosen in each case. It normally consists of chemical reactions that can be described as radical

View Article Online
DOI: 10.1039/C7GC02009K

polymerization within the NE droplets and needs an initiator (*e.g.*, radicals formed during ultrasonic cavitation).[7] MCs generally refer to hollow spherical structures which can host, and eventually protect, an active molecule. The presence of oil as a template or core for the capsule formation can also ease the dissolution of poorly soluble drugs or lipophilic actives.[8,9] MCs are ideally made form a non-toxic, biodegradable polymer consisting of an amphiphilic backbone that gives the possibility to bind equally efficiently to the hydrophobic core and cover it, but also to have a high affinity to water and be water dispersible. This will in principle ease, *e.g.*, the protected delivery of water insoluble drugs.

Recently the use of natural polyphenols in form of lignins has been proposed as an innovative shell for nanocapsule (NC) synthesis.[10,11] The polyphenolic nature of the shell in fact provides unique antioxidant, complexing and pH responsive properties.[12,13] [10]

Tannins are natural polyphenols found in most of higher plants around the globe.[14] They play a significant role in defending the plant against insects, infections, fungi or bacteria; this role stems from their capability to form complexes with proteins, polysaccharides and metals, and hence provide protection of the vulnerable parts of the plants from invasive microbial extracellular enzymes.[15,16,17] Tannins are classified according to their structure and reactivity into hydrolysable, non-hydrolysable and complex species (**Figure 1**).[15] Hydrolysable tannins are esters of gallic acid with a core sugar, often glucose. Tannic acid is the most prominent representative of the family of hydrolysable tannins.[18] Condensed tannins are oligomeric and polymeric proanthocyanidins consisting of flavan-3-ol units, linked by carbon-carbon bonds not susceptible to hydrolytic cleavage.[19,20,21,22] The scaffold of the subclass of tannins called complex

View Article Online
DOI: 10.1039/C7GC02009K

tannins is very similar to that found in condensed and hydrolysable tannins, where a flavan-3-ol unit is linked to gallic acid in a monomeric or polymeric system.[23]

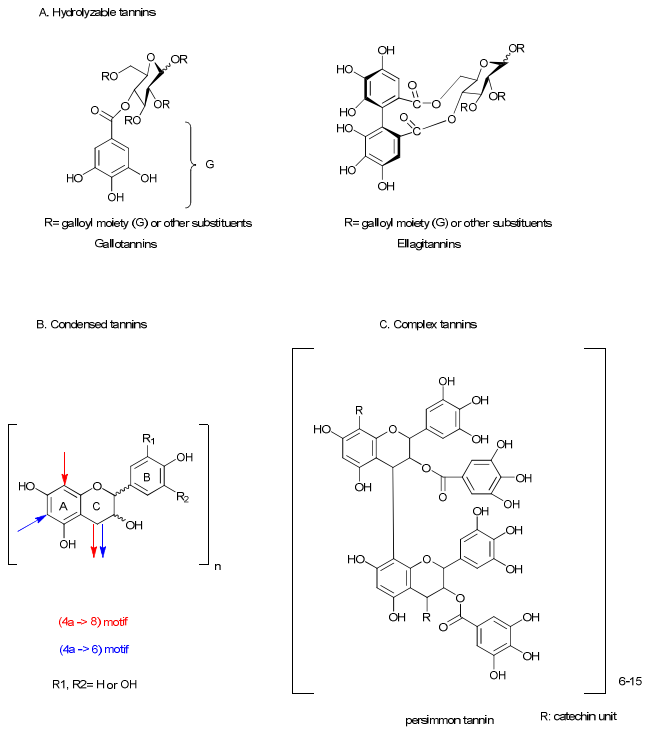

Figure 1: Classification of tannins. For details refer to main text.

Tannins are present in significant amount (up to 30%) in barks and plant residues. However, their exploitation as renewable high added value products is to date not extensive and limited mainly to bulk and low-values industrial utilization,[24,25,26] despite their interesting intrinsic properties including high biocompatibility and biodegradability,[27] UV-light absorption ability[28] and complexation capabilities against numerous other elements and molecules besides proteins.[29]The fundamental positive health effects of tannins[30,31,32,33,34] that are connected to their high antioxidant activity and their role as radical scavengers that allows for protection from

View Article Online
DOI: 10.1039/C7GC02009K

diseases associated with the presence of free radicals in the body, such as cancer, arthritis, degenerative eye and neurological disorders undoubtedly reveal an intriguing potential for applications in the biomedical field that has yet to be explored.

With the aim of developing new functional active delivery systems with unique stimuli responsive properties, the possibilities emerging from tannins as shell materials were to be exploited in view of their: (a) biocompatibility, (b) antioxidant activity to protect the active; (c) potentially relevant biological activity to exert synergistic effect with the active; (d) self-aggregation tendencies, and (e) amphiphilic characteristics. The tannin backbone is comprised of aromatic rings carrying phenolic moieties, resulting in a backbone with high tendency to undergo intermolecular attractions unique to aromatic moieties that have proven essential for the ultrasound based generation of nanocapsules.[10,35]

Low molecular weight specific tannins (such as the gallic acid or different catechin units)[36,37,38,39], have been used as stabilizers[40] or bioactive NEs,[38,41] or, alternatively, as additives to provide an efficient barrier against moisture, gas and solutes in the development of brittle films.[36] The properties of tannins as stabilizers and barrier agents, associated with their antioxidant activity and their role in increasing hydrophobic interactions within different sites in proteins[42] as well as in enhancing the functional properties (*i.e.*, resistance and flexibility) of fabricated biodegradable films[36]make this class of polyphenols a unique unprecedented starting material for the development of structured and stable capsules & emulsions for controlled, stimuli responsive delivery of actives.[43]

In this work, an easy and straightforward ultrasound based approach for the fabrication of MCs and NEs based on different tannin scaffolds, namely two commercially available condensed tannin samples: *Schinopsis balansae* wood extract (***Sb***), *Acacia mearnsii* bark extract (***Am***);

View Article Online
DOI: 10.1039/C7GC02009K

commercial tannic acid (**TA**) and a purified green tea extract consisting in epigallocatechin-3-*O*-gallate (96%) (**EGCG**),[20,21,22] in the absence of cross-linking agents is reported. The synthesis of capsules by sonication further constitutes an economically viable and environmentally benign approach to encapsulation that allows also easy tuning of the parameters in order to modify the nanostructure dimensions.[44,45] Advantages of the selected methodology are associated to the short reaction times and the narrow size distribution of the resulting particles.[46,47,48]

.

EXPERIMENTAL SECTION

Materials

Schinopsis balansae wood extract (***Sb***), *Acacia mearnsii* bark extract (***Am***), were obtained by Silvachimica s.r.l. (Italy). Tannic acid (**TA**), Coumarin 6, highly refined olive oil of low acidity and mineral oil were purchased from Sigma Aldrich and used as received. Epigallocatechin-3-*O*-gallate in form of purified green tea extract was purchased in a conventional pharmacy. All other reagents and solvents were purchased from Sigma Aldrich in appropriate grads and used as received, if not stated otherwise.

One step assembly of tannin microstructures (TMSs) by sonication

Emulsions of olive oil in polyphenol solutions were prepared according to the method previously developed by Crestini *et coll*,[10] by dispersing 0.1 mL of either olive oil or mineral oil in 1.0 mL of 0.5% (w/v) solution in aqueous MOPS buffer (0.1 M, pH 7.4) (for ***Sb*** and ***Am***) or 0.25 % (w/v)

View Article Online
DOI: 10.1039/C7GC02009K

solutions in aqueous MOPS buffer (0.1 M, pH 7.4) (for **TA** and **EGCG**) at pH 7.4 and sonicating as follows: applying in principal an acoustic power of 160 W, for 40 seconds, using a 3 mm diameter microtip connected to a 20 kHz Branson probe (Branson Digital Sonifier by Ultrasonic Corporation, Model 450L).

Isolation of the tannin microcapsules (TMCs) and tannin nanoemulsions (TNEs)

In case of ***Sb*** and ***Am*** TMCs, separation and washing of the capsules was realized by centrifugation of the sonicated samples at 5000 rpm for 5 minutes for the. The lower part corresponding to the tannin residues was removed and the foamy supernatant consisting in microcapsules was washed twice with 1.0 mL of distilled water. The different washing solutions were combined for further analysis.

In case of **TA** and **EGCG**, *i.e.*, when no phase separation was observed, the NE was left as obtained after the sonication for further analysis.

Characterization of tannin microstructures

Optical and fluorescence microscopy analysis

The isolated MCs and NEs were diluted with distilled water to yield a suspension in water at a final dilution of 1/10. An aliquot was analysed by microscopy. In case the droplets overlapped and thus impaired the subsequent image analysis, the sample was further diluted. A Zeiss microscope was used and all images were obtained with10 x, 40 x, 63 x and 100 x objective lens magnification.

View Article Online
DOI: 10.1039/C7GC02009K

Statistical quantitative analysis of capsules

The microscopy images were processed using the image analysis software ImageJ combined with Excel-based analysis to obtain a statistical summary of yields (expressed in number of nanocapsules/mL), mean diameters incl. standard deviations and polydispersion indices, as described previously.[10] In order to have statistical relevant results in terms of nanocapsule numbers, the three qualitatively best images were chosen for the Software-based Image J analysis.

Shell size analysis.

Analysis of the shell dimensions of the samples was carried out as described in detail before for lignin-based capsules.[10] In short, tannins were labelled with fluorescein isothiocyanate (FITC) by reacting 10 % of the free aromatic hydroxyl groups of the starting tannins in dry DMF (determined *via* quantitative ^{31}P NMR data as described below) prior to capsule formation. The resulting FITC-functionalized tannins were washed with a minimum amount of distilled water until the characteristic yellow colour of FITC was no longer evident in the residual aqueous solutions. Workup in case of **EGCG** consisted in a liquid-liquid extraction in ethyl acetate (EtOAc) and removal of the solvent *in vacuo* to yield the solid FITC-labelled **EGCG**. Capsules were formed following the general procedure outlined above by sonicating an o/w emulsion consisting in 1.0 mL of a 0.25-0.5 % w/v aqueous solution depending on the labelled tannin and 0.1 mL of a non-fluorescent mineral oil as the hydrophobic template. The shell thickness was estimated from the fluorescent contour of the capsules in fluorescent microscopy analysis.

View Article Online
DOI: 10.1039/C7GC02009K

Cryo-SEM

Cryo-SEM analyses were performed using a QuorumPP-2000T cryo-preparation system installed at a FEI Helios 600 Dual beam machine. Sample preparation and measurements were performed as described in detail before.[10]

pH stability studies

The pH responsiveness of the capsules was evaluated using *Acacia mearnsii* tannin (***Am***T). generated by ultrasonication as described above starting from an aqueous solution of ***Am***T inMOPS buffer at pH 7.4. MC formation was repeated 10 times and capsules were isolated in 10 small Eppendorf tubes. The pH was carefully adjusted throughout a pH range between 2-12 by changing one unit at a time using diluted aqueous hydrogen chloride and diluted aqueous sodium hydroxide. Capsules were observed for eventual macroscopic changes in their consistency and were analysed *via* optical microscopy for statistical analysis as described above.

Tannin characterization

The tannin characterization consisted in the determination of the distribution of molecular weights by means of gel permeation chromatography (GPC) and in the ^{31}P NMR analysis of the different phenolic groups contained in the specific tannin sample. The treatment for the isolation of both types of tannin (the tannin of the capsule shell and the fraction found in the washing solution) involved lyophilisation and subsequent extraction of the samples with *n*- hexane.

Gel Permeation Chromatography (GPC).

Approx. 3.0 mg tannin was suspended in 1.0 mL glacial acetic acid/acetyl bromide (9:1 (v/v)) for 2 h in accordance with the method provided for lignins by Asikkala *et al*.[49]The solvent was then

View Article Online
DOI: 10.1039/C7GC02009K

removed under reduced pressure, and the residue was dissolved in HPLC-grade THF and filtered over a 0.45 µm syringe filter prior to injection. GPC-analyses were performed as described before[10] using a Shimadzu instrument consisting of a controller unit (CBM-20A), a pumping unit (LC 20AT) equipped with a 20 µL sample loop, a degasser unit (DGU-20A3), a column oven (CTO-20AC), a diode array detector (SPD-M20A), and a refractive index detector (RID-10A); Shimadzu LabSolution software package (Version 5.42 SP3) was used for control. Three analytical GPC columns (each 7.5 x 30 mm) were connected in series for analyses: Agilent PLgel 5 µm 10000 Å, followed by Agilent PLgel 5 µm 1000 Å and Agilent PLgel 5 µm 500 Å. Calibration was performed with polystyrene standards (Sigma Aldrich, MW range 162 - 5 x 10^6 g mol^{-1}). Final analyses of each sample was performed as described elsewhere[50]

^{31}P NMR

^{31}P NMR analysis was performed after derivatization of accurately weighed lignin samples (20-25 mg) with the reagent 2-chloro-4,4',5,5'- tetramethyl-1,3,2-dioxaphospholane, according to methods previously published,[51,52,21,22] using an inverse-gated pulse-sequence on either a Bruker 300 MHz or a Bruker 700 Mhz NMR spectrometer, controlled *via* TopSpin software packages.

Active loading measurement- Encapsulation efficiency (EE)

Encapsulation studies were performed using Coumarin 6 as fluorescent probe. For the preparation of the primary emulsion, 0.1 mL of a solution of Coumarin 6 in olive oil (0.2 mg/ mL) was added to 1.0 mL of a solution of tannin in MOPS; the resulting o/w suspension was sonicated as described above. The systems obtained were isolated depending on their capsule or emulsion nature as described above.

View Article Online
DOI: 10.1039/C7GC02009K

The encapsulation efficiency of the TMCs and TNEs was determined spectrophotometrically *via* UV-vis analysis at an absorbance maximum 463 nm, applying a direct loading study of the capsules and an indirect study of the washing solutions in the case of isolated TMCs, and a study of the total volume of the nanoemulsion in case of TNEs. Spectra were obtained using a ShimadzuUV-vis spectrophotometer UV 1800.

Direct loading studies: The total volume of Coumarin 6 loaded TMCs and TNEs of three different sets of preparations were disassembled by addition of $CHCl_3$ and subsequent immersion in an ultrasonic bath. The organic phase was removed every 15 minutes and fresh solvent was added. The procedure was repeated three times to ensure that the foam was discoloured. The organic phases were reunited and left to dry overnight. The dry sample was re-dissolved in 2.0 ml of $CHCl_3$ and the amount of the extracted Coumarin 6 was quantified based on a calibration using a set of differently concentrated solutions of Coumarin 6 in $CHCl_3$.EE_{direct} was determined as follows:

$$EE_{direct} = \frac{\text{released Coumarin 6}}{\text{initial Coumarin 6}} \text{x}100$$

Indirect loading studies were performed by analysing the aqueous washing solutions obtained during TMC work-up. The aqueous suspension obtained by mixing the washing residues with an excess of $CHCl_3$ was centrifuged at 5000 rpm during15 min. The bottom phase was collected and was left to dry , and the dried sample was re-dissolved in 2.0 ml of $CHCl_3$ before the quantitative analysis *via* UV-vis analysis for Coumarin 6 as described above. $EE_{indirect}$ was calculated as follows:

$$EE_{indirect} = \frac{\text{Initial Coumarin 6} - \text{ quantified Coumarin 6}}{\text{Initial Coumarin 6}} \text{x}100$$

View Article Online
DOI: 10.1039/C7GC02009K

The quantities of Coumarin 6 determined by direct and indirect studies are expressed in percentages found in the capsules or the washes with respect to the initial concentration of the added Coumarin 6. The loaded amount of the Coumarin 6 is finally expressed as attograms (ag) per capsule, taking into consideration also the statistical quantitative measurements of each sample.

Release kinetics

In vitro release of the encapsulated hydrophobic active, *i.e.*, Coumarin 6, was studied as follows in aqueous phosphate saline buffer (PBS) (0.1 M) at pH 7.4,applying a protocol that consisted in quantifying the amounts of the active released at designated times *via* UV-vis spectroscopy on the basis of a calibration curve at an absorbance maximum of $\lambda = 463$ nm. The aliquots were lyophilized and the resulting samples were dissolved in 1.0 mL of $CHCl_3$ and centrifuged to remove the salts before the UV-vis measurement of the clear $CHCl_3$ supernatant. The analysis was performed as follows: 1.0 ml of PBS aqueous solution was added to the isolated Coumarin 6-filled TMCs (~0.1 mL) or TNEs (1.0 mL) and the resulting suspension was left under gentle agitation at 25°C. At fixed intervals (0, 30 min, 1 hour (h), 2 h, 4 h, 8 h, 24 h, 2 days (d), 3 d, 5 d, 7 d, 8 d, 9 d, 10 d) the sample was centrifuged at 5000 rpm for 5 min and intake amounts of Coumarin6 in the aqueous loaded TMCs were isolated from the supernatant foam. The remaining foam after each separation was dispersed in 1.0 mL of SDS and left under gentle shaking. The procedure was continued until no peak attributable to Coumarin 6 was detected in the UV spectrum. The results of this type of analysis were processed based on the absorbance of the aliquots at the λ_{max} of Coumarin 6 and the quantified amount was added to the amount of Coumarin 6 found in the analysis of the previous time point yielding to the release percentage

View Article Online
DOI: 10.1039/C7GC02009K

that was normalized to the maximum amount of Coumarin 6that was efficiently released after 10 days.

The Coumarin 6 that was not released after the 10^{th}day, was finally released after the complete disassembly of the system in $CHCl_3$.

Genotoxicity studies

General: Chinese hamster ovary (CHO) cells were obtained from Sigma-Aldrich. Stocks of CHO cells are stored in liquid nitrogen and subcultures are prepared from these stocks for experimental use. Cultures were grown as monolayer cultures in Ham's F-10 medium (Gibco BRL) supplemented with 15% foetal bovine serum, 4mM*L*-glutamine and antibiotics (50 IU/mL penicillin and 50 IU/mL streptomycin). All incubations were at 37 °C in a 5% carbon dioxide atmosphere and 100% nominal humidity. Approximately 24 hours before treatment exponentially growing cells were detached by trypsin action and an appropriate number of 25 cm^2 plastic cell culture flasks containing 5 mL complete culture medium was individually inoculated with 3.0×10^5 cells for each assay performed.

Chromosomal aberration assays

Treatment with the test compounds was performed for 3 and 21 hours and cells were harvested at 21 hours from the beginning of the treatment (approximately 1.5 cell cycle length). At the end of the 3 hour treatment, cultures were washed twice with Ca/Mg-free Phosphate Buffered Saline (PBS) solution and re-incubated at 37° C in fresh complete culture medium for a further 18 hours, until harvest. Cultures received also 5-bromo-2'-deoxyuridine, 9.8 μM to permit sister chromatid differentiation and allow the analysis of cell cycle progression. Colcemid at 0.27 mM

View Article Online
DOI: 10.1039/C7GC02009K

was added during the last 3 hours of culture to accumulate cells in metaphase. Hypotonic shock was induced by 1% trisodium citrate solution for 10 minutes. Cell suspension was fixed in a mixture of methanol and glacial acetic acid (v/v 3:1) followed by three washes. Cytogenetic preparations for analyses of chromosomal aberrations and mitotic indices were stained with an aqueous solution of Giemsa (3%).Solvent-treated cells served as negative control. The mitotic index was expressed in percentage based on the number of metaphases present after a total of 1000 cells scored (interphases and metaphases). The frequencies of M_1, M_2 and M_3 were determined by scoring 100 metaphases for each culture and the proliferation index (PI) was calculated according to equation:

$$PI = (1 \times M_1 + 2 \times M_2 + 3 \times M_3) / \text{total number of metaphases.}$$

For each experimental point, 100 metaphases were scored for chromosomal aberrations and were classified according to the description of Savage.[53] The numbers of cells bearing aberrations (excluding gaps) in the negative control and treated cultures were compared using Fisher's exact test.[54]

Micronucleus assay

A continuous treatment with TMC was performed for 24 hours, corresponding to approximately 2 cell cycle length. Cytochalasin B at the final concentration of 3 µg/mL was added together with the test compounds. At the end of treatment the cells were brought into suspension with a trypsin solution and centrifuged. The cell pellets were resuspended in hypotonic solution and fixed in

View Article Online
DOI: 10.1039/C7GC02009K

fresh methanol. Cytogenetic preparations from these cultures were obtained following standard procedures and slides stained in 3% aqueous solution of Giemsa.

The cytokinesis-block proliferation index (CBPI) was used to calculate cytotoxicity by the following formula:

$$\% \text{ Cytotostasis} = 100 - 100\,[(CBPI_T - 1) / (CBPI_C - 1)]$$

with:

$$CBPI = (\#\text{ mononucleated cells} + 2 \times \#\text{ binucleated cells} + 3 \times \#\text{ multinucleated cells}) / \text{total number of cells}$$

CBPI was determined from at least 500 cells per culture. At least 1000 binucleated cells per culture were scored to assess the frequency of micronucleated cells. The criteria for identifying micronuclei have been described by Kirsh-Volders *et al*.[55] The numbers of binucleated cells with micronuclei in the control and treated cultures were compared using a $\chi 2$ calculation.[56]

Comet assay[57]

Treatment with the test compounds was performed for 3 hours. At the end of treatment the cells were brought into suspension with a trypsin solution and centrifuged. Approx. 10 µL of each cell suspension was added to 65 µL of 0.7% (w/v) low melting point agarose (Bio-Rad Lab) and sandwiched between a lower layer of 1% (w/v) normal-melting agarose (Bio-Rad Lab). For each

View Article Online
DOI: 10.1039/C7GC02009K

compound, two sets of three slides each, were prepared. The slides were kept at +4°C for 5 minutes and then immersed in aqueous lysing solution (2.5 M NaCl, 100 mM Na_2EDTA, 10 mM Tris, pH 10) containing 10% DMSO and 1% Triton x 100 (ICN Biomedicals Inc.) at 4°C overnight. Slides were then randomly placed in a horizontal gel electrophoresis apparatus with fresh alkaline electrophoresis buffer (300 mM aqueous NaOH, 1.0 mM Na_2EDTA, pH > 13) and incubated for 25 min at 4°C to allow for DNA unwinding and expression of alkali-labile sites. Electrophoresis was at 4°C for 15 minutes at 30 V (1 V/cm) and 300 mA. After electrophoresis, slides were immersed in 0.3 M sodium acetate in ethanol for 30 min. Slides were then dehydrated in an alcohol series (2 min at 70, 85, and 100%) and air-dried. Slides stained with 20 µg/mL ethidium bromide in the presence of antifade immediately before analysis, were examined at 40X magnification using an automated image analysis system (Comet Assay III; Perceptive Instruments, UK) connected to a fluorescence microscope (Zeiss Axioskop 2). DNA damage was quantified from the % tail intensity values. A number of 50 cells from each slide (150 cells in total) were analysed per experimental point. To determine the statistical significance of DNA damage induction, the % tail intensity values in the solvent control and treated cultures were compared using the Student's t-test.[58]

RESULTS AND DISCUSSION

One step assembly of tannin microstructures (TMSs) by sonication

With the objective to explore the opportunities in the ultrasound-based synthesis of tannin microstructures two different condensed tannins were selected for microcapsule (MC) assembly: *Schinopsis balansae* wood extract (***Sb***) and *Acacia mearnsii* bark extract (***Am***). The study of

View Article Online
DOI: 10.1039/C7GC02009K

nanoemulsion (NE) assembly and behaviour was carried out on the hydrolysable tannins *tannic acid* (**TA**) and epigallocatechin-3-*O*-gallate (**EGCG**), in view of their reduced molecular weight with respect to condensed tannins. **Figure2** shows the specific structures of the selected tannins.

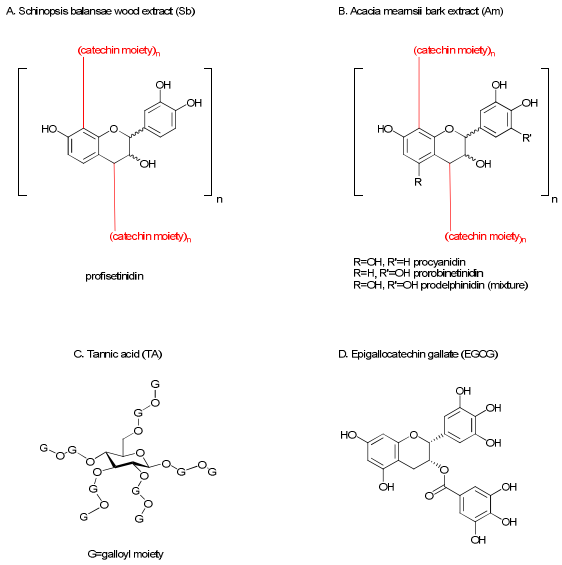

Figure 2: A. Structure of ***Sb***T, assigned as a profisetinidin; B: structure of ***Am***T, assigned as mainly being prodelphinidin; C: **TA**; D: **EGCG**.

The amount and distribution of the phenolic groups in these tannins and their detailed structure were determined *via* ^{31}P NMR analysis as recently reported.[20] More specifically, the overall phenolic contents were found to be 7.7 mmol/g for ***Sb***, 8.9 mmol/g for ***Am***, 16.4 mmol/g for **TA** and 19.0 mmol/g for **EGCG**.(**Table 1**).

Table 1: Number average molecular weight (Mn) and total phenolic-OH content of ***Sb***T, ***Am***T, **TA** and **EGCG**) as evaluated by GPC analysis and quantitative ^{31}P NMR spectroscopy, respectively.

Tannin	Number average molecular weight (Mn)	Total phenolic-OH

View Article Online
DOI: 10.1039/C7GC02009K

	[Da]	[mmol/g]
Sb	1000	7.7
Am	960	8.9
TA	1300	16.4
EGCG	500	19.0

Further detailed structural characterization has been carried out in a previous effort by HSQC analysis:[20] ***Sb***T was identified as a profisetinidin and ***Am***T was shown to consist mainly of prodelphinidin, with minor amounts of prorobinetinidin and procyanidin present (**Figure 2**). These two tannins were chosen since they display different oxidation patterns on the rings A and B (catecholic and pyrogallolic on the one hand, and phlorglucinolic and resorcinolic on the other hand) that in principle display different complexing properties.

The potential of different tannins to form nanostructures was examined by applying standard conditions of sonication and isolation concerning sonication time (40 s), temperature (30 °C), sonication probe (3 mm Tip), cavitation region (surface contact area calculated as a ratio between the surface of the sonication probe and the small vessel 25% for tip/Falcon tube) and speed of centrifuge (5000 rpm) based on general optimization studies described in previous works.[10] Two characteristic sonication power values of 40 and 160 W were screened for low and high acoustic intensity, respectively. The formation of sub-micrometre and NEs was accomplished by the use of high frequency ultrasound that was proven to lead to the formation of stable emulsions as reactor initiators that afterwards led to the formation of core-shell colloidal microdroplets. [59,60]

NEs based on green tea catechins had been previously reported to be formed by high shear and high pressure homogenization processes.[61] More specifically, **EGCG** has been reportedly used

View Article Online
DOI: 10.1039/C7GC02009K

as the encapsulated active or as an additive for the generation of stable NEs in food industry.[62] In such studies, however, **EGCG** has not been used as the principle capsule shell component, but together with active substances, sunflower or palm oil and a combination of emulsifiers.

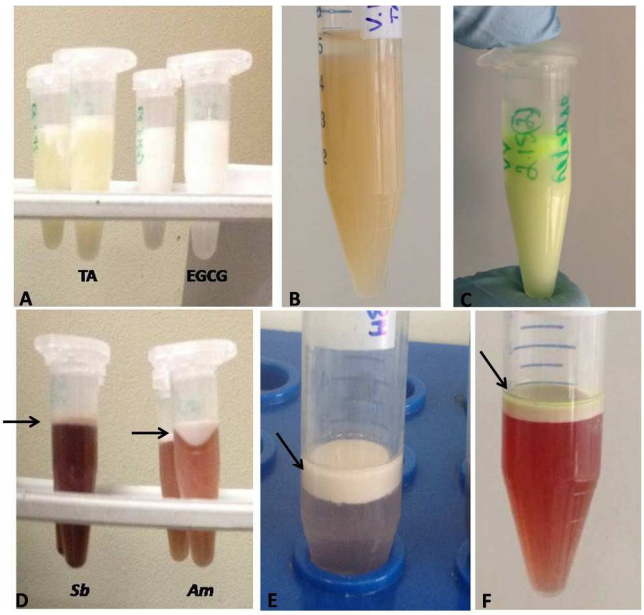

Figure 3: A. Macroscopic image of NEs made of **TA** and **EGCG** microdroplets; B: destabilization of **TA** NE after standard isolation protocol *via* centrifugation; C: Coumarin 6-loaded **EGCG** NE; D: macroscopic image of ***Sb***- and ***Am***- TMCs; E: isolated ***Am*** TMCs stable after centrifugation; and F: Coumarin 6-filled ***Am*** TMCs.

In the present study, **EGCG** and **TA** were used as the shell matrices. Aqueous MOPS solution was chosen as the buffer primarily to enhance the tannin solubility issues; nevertheless, it may have also contributed to the emulsion formation playing the role of emulsifier.

The concentration of the tannin solutions to sonicate was adjusted in order to have a constant amount of phenolic OH-groups in solution (approx.. 40 mmol / mL) based on the amounts revealed by quantitative ^{31}P NMR. As such a 5 mg / mL was used for ***Am*** and ***Sb*** tannins, while a concentration of 2.5 mg / mL was used for **TA** and **EGCG**.

View Article Online
DOI: 10.1039/C7GC02009K

Sonication of **TA** and **EGCG** in an o/w suspension led to the formation of white NEs (**Figure 3A**) with partially stable droplets. Due to their labile nature, during centrifugation, NEs underwent phase separation (**Figure 3B**). Nevertheless, they showed no sign of creaming, when kept still or under gentle stirring for over a month. In a second experiment, sonication of **TA** and **EGCG** was carried out in the presence of Coumarin 6 as a fluorescent probe for active upload studies. The NEs formed by **TA** and **EGCG** showed a distribution of the Coumarin 6 throughout the total volume of the emulsion (**Figure 3C**).

On the contrary, analogous experiments showed efficient formation of capsules for all the condensed tannins, i.e., ***Sb*** and ***Am***, as shown in **Figure 3D**, as an upper foam. The different consistency of the systems (NEs *vs.* MCs) was further confirmed upon centrifugation and subsequently after the addition of Coumarin 6 in the hydrophobic core. Unlike TNEs, TMCs were stable after centrifugation (**Figure 3E**) and efficiently incorporated the hydrophobic active inside the foamy supernatant (**Figure 3F**).

Figure 4 shows the optical microscopy images of ***Sb*** and ***Am*** TMCs formed at 40 and 160 W.

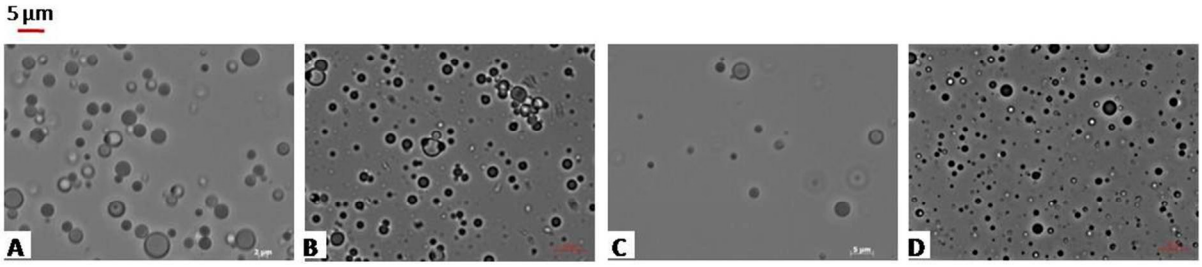

Figure 4: Optical microscopy images: A: ***Sb*** TMCs formed at 40 W; B: ***Sb*** TMCs formed at 160 W; C: ***Am*** TMCs formed at 40 W, and D: ***Am*** TMCs formed at 160 W (scale bar 5 µm).

TMCs formed at low power are significantly bigger (ca 2 µm) compared to the capsules generated at high power (mean size ca 0.7 µm). Furthermore, the capsules generated at high power were obtained in higher yields (see **Table 2**, entry 2).

View Article Online
DOI: 10.1039/C7GC02009K

The **TA** and **EGCG** TNEs were formed at low (40 W) and high sonication power (160 W). **Figure 5** shows the optical microscopy analysis performed on the obtained samples.

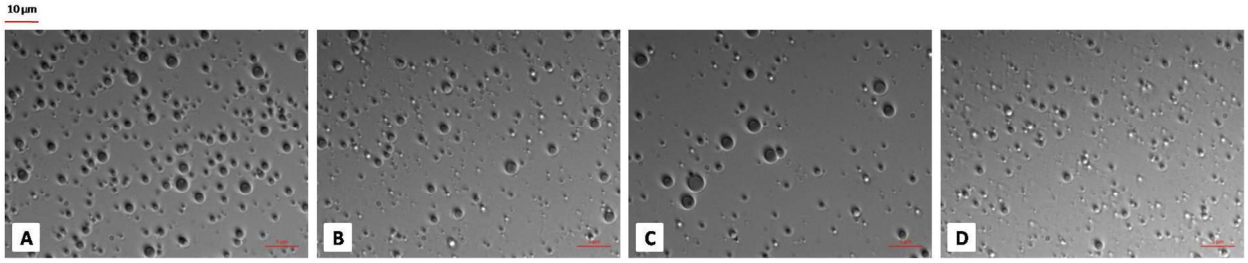

Figure 5: Optical microscopy images: A:**TA** NE formed at 40 W; B: **TA** NE formed at160 W; C: **EGCG** NE formed at 40 W; and D: **EGCG** NE formed at 160 W (scale bar 10 µm).

The size of the spherical droplets did not vary substantially upon increase of sonication power, as shown below in **Figure 6**. This property of the NEs is different compared to the properties of previously analysed MCs based on the condensed tannins ***Am*** and ***Sb***.

Characterization of tannin microstructures

Morphological characterization of the colloidal systems

In order to elucidate the morphology of the capsules, cryo-SEM analysis of the various samples was performed. The cryogenic technique was preferred due to the delicate liquid nature of the systems that appear to be unstable under the vacuum conditions of the standard SEM experiments. Furthermore, using this technique, the sample could be viewed with an increased resolution capability in its fully hydrated state where it retains its conformation.[63] **Figure 6** shows the cryo-SEM images of the ***Sb*** TMCs generated at 40 W.

View Article Online
DOI: 10.1039/C7GC02009K

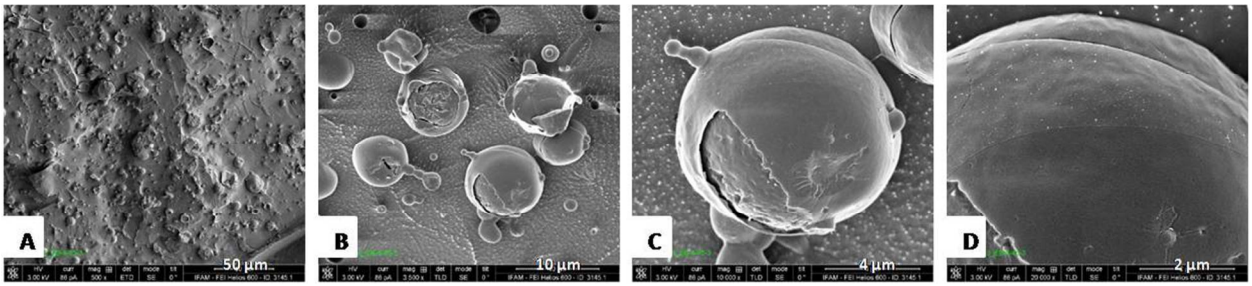

Figure 6: Cryo-SEM analyses: A: ***Sb*** TMCs formed at 40 W; B and C: distinct core-shell nature of TMCs; and D: smooth morphology of the tannin capsule shell.

TMCs consist of spherical capsules of average 2 µm diameter that show a clear distinction between the core and the shell. The sizes of the capsules are in agreement with the optical microscopy analysis made for ***Sb*** TMCs formed by low acoustic power as shown in **Figure 4A**. The detailed size analysis of the capsules is reported in **Table 2**.The olive oil template is evident; playing the role of the hydrophobic core of the capsule it acts as the liquid reservoir for lipophilic actives, whereas the outer coating, i.e., the ***Sb***T, appears as a relatively thick shell wall (0.15-0.3 µm thickness), which determines the dispersion stability and controls the release characteristics of the system (see **Table 2** for detailed analysis).

Shell size analysis

Shell size determination was carried out by labelling of tannins with a fluorescent marker prior to sonication of typical o/w emulsions prepared thereof and subsequent microscopy analysis of obtained TMCs.

10% of the free phenolic OH-groups (as determined by quantitative ^{31}P NMR analysis) of the tannins were functionalized with fluorescein isothiocyanate (FITC) to yield highly fluorescent tannins. The efficient isolation of the tannins from the residual FITC required several washes and centrifugation cycles. A non-fluorescent mineral oil instead of the naturally slightly fluorescent default olive oil was used for the preparation of the FITC-labelled capsules. The systems were

View Article Online
DOI: 10.1039/C7GC02009K

observed by optical and fluorescence microscopy. The fluorescence analysis revealed spherical droplets with a non-fluorescent dark core that are surrounded by a green fluorescent contour (**Figure 7A**,**C**, **E** and **G**). These results together with the cryo-SEM experiments give a fundamental structural understanding of the colloidal systems and further prove their capsule nature.

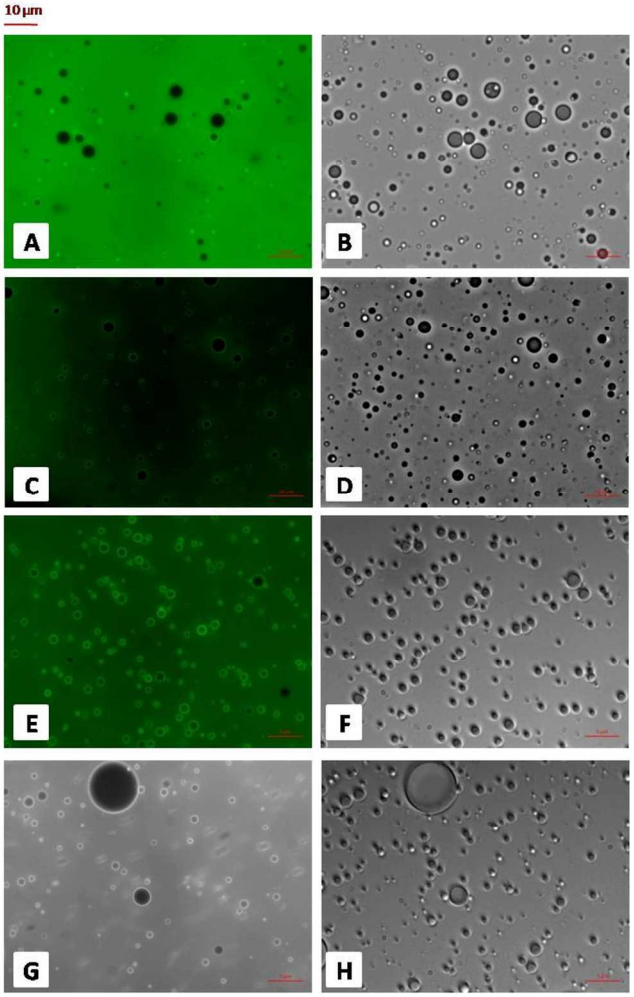

Figure 7: Fluorescence (left) and optical (right) microscopy image: A and B: FITC-***Sb*** TMCs; C and D: FITC-***Am*** TMCs; E and F: FITC-**TA** NE; and G and H: FITC-**EGCG** NE (scale bar 10 µm).

The slightly fluorescent background is due to the incomplete washing of the excess of FITC from the functionalized tannins, prior to capsule formation. The images clearly depict the fluorescence

View Article Online
DOI: 10.1039/C7GC02009K

coming from the functionalized tannin shell to be significantly more intense than the background, thus allowing for reliable shell analysis. The micro-and nanostructures that were formed from the sonication of various tannins did not show significant microscopic differences in the microscopy analysis, not even when labelled; all of them revealed a core-shell nature that could be used for the efficient transfer of active substances.

The shell size analysis was performed manually using the ImageJ software by determining the fluorescent outline of the droplets; the average values calculated are reported in **Table 2**.

Encapsulation of actives

The encapsulation potential of the colloidal systems was investigated using the fluorescent probe Coumarin 6. Tannin capsules from ***Sb*** and microdroplets from **TA** were generated in the presence of Coumarin 6 by sonication at 160 W. **Figure 8** shows the optical and fluorescence microscopy images of the obtained systems. Coumarin 6 (green) is located in the capsule core of ***Sb*** TMCs and of the droplets of the **TA** NE. The active appears to be uniformly distributed within the capsules and NE droplets. This is a critical factor for the subsequent uniform active release from the capsules once they are administered *in vivo*.

View Article Online
DOI: 10.1039/C7GC02009K

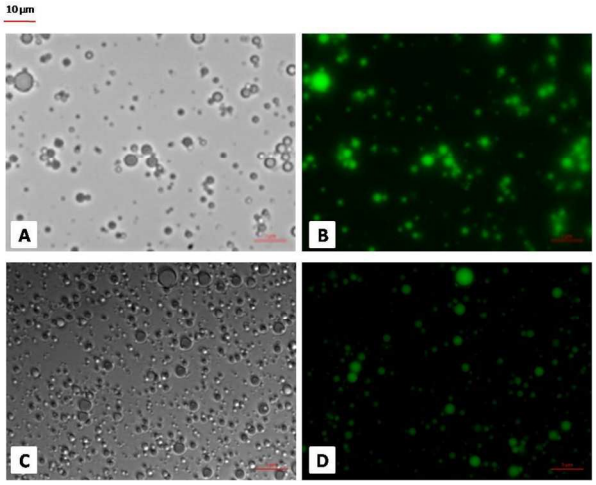

Figure 8: Optical and fluorescence microscopy of Coumarin 6-filled TMCs and TNEs: A and B. ***Sb*** TMCs; and C and D: **TA** NE droplets (scale bar 10 µm).

Statistical quantitative analysis

Table 2 reports the various characteristic values representative of the size distribution of the different systems under study, including average diameter of the droplets, minimum and maximum sizes observed for each system and the polydispersity, [64] *i.e.*, the division of standard deviation by mean diameter evaluated by the statistical analysis of the ImageJ-processed images. Furthermore, the yield of the efficient droplet formation is reported and is expressed in number of droplets or microcapsules/mL (MCs/mL) for each system, whereas the absolute yield corresponds to the number of droplets or microcapsules that were formed in the actual volume that was isolated and is calculated based on the different volumes that were isolated for MCs and NEs, *i.e.*, 0.1 mL for upper foam that consists of MCs, but 1.1 mL for the NEs, since it contains the total volume used initially for the preparation and no isolation steps have intervened.

View Article Online
DOI: 10.1039/C7GC02009K

Table 2: Size distribution analysis and loading potential for *Schinopsis balansae* (***Sb***), *Acacia mearnsii* tannin (***Am***), tannic acid (**TA**) and epigallocatechin-3-*O*-gallate (**EGCG**) based micro-structures

Entry	Tannin	Sonication power (W)	Mean Ø (μm)	Pd	Min-max Ø (μm)	Yield (MCs/mL)	Absolute yield (MCs)	Shell size (μm)	EE(%)	Absolute EE (ag/droplet)
1	***Sb***	40	1.8	0.5	0.4-5.2	$5.1x10^{9}$	$5.1x10^{8}$	0.31	n.d.[a]	
2	***Sb***	160	0.6	0.3	0.4-1.1	$2.1x10^{11}$	$2.1x10^{10}$	0.14	77±3	743
3	***Am***	40	1.4	0.4	0.5-4.1	$2.4x10^{9}$	$2.4x10^{8}$	0.25	n.d.[a]	
4	***Am***	160	0.7	0.3	0.4-1.2	$9.3x10^{11}$	$9.3x10^{10}$	0.13	72±8	155
5	**TA**	40	0.7	0.5	0.5-2.1	$7.3x10^{11}$	$7.3x10^{11}$	0.15	n.d.[a]	
6	**TA**	160	0.5	0.6	0.2-1.8	$7.6x10^{11}$	$7.6x10^{11}$	0.12	100±1	26
7	**EGCG**	40	0.7	0.7	0.2-2.1	$3.3x10^{11}$	$3.3x10^{11}$	0.17	n.d.	
8	**EGCG**	160	0.6	0.5	0.2-2.5	$6.8x10^{11}$	$6.8x10^{11}$	0.17	99±2	29

[a:] Pd: polydispersity; EE: encapsulation efficiency; ag: attograms.
[b:] Encapsulation efficiency determined only for the optimised system with enhanced features of increased sonication power.

As reported in **Table 2**, the spherical microstructures were obtained in high yields independently of the conditions of sonication. Capsule generation upon ultrasonic treatment comes as a result of the numerous physicochemical processes that are initiated by the extreme conditions induced by the acoustic power. When increased sonication power levels are applied, the generated capsules are generally of smaller sizes with a narrower distribution as implied by the low polydispersity indices (**Table 2**, entries 2, 4, 6, 8). This is expected as a trend, since the alteration of the sonication amplitudes is a commonly used factor to tune the characteristics of the systems generated upon sonication.[65,66] It is noteworthy that in the case of the NEs formed from **TA** and **EGCG**, the sizes of the systems did not vary significantly (**Table 2**, entries 5-8).

The condensed tannins ***Sb*** and ***Am*** show a comparable trend in size distribution and form capsules of 1-2 μm upon low power sonication (**Table 2**, entries 1, 3). From the total and absolute yields it can be concluded that for the condensed tannins ***Sb*** and ***Am***, the increase of sonication power results also in the increase of the number of capsules formed (**Table 2**, entries

View Article Online
DOI: 10.1039/C7GC02009K

2, 4). The increase in yield and decrease in sizes and shell dimensions are in accordance with the sonication theory. More specifically, smaller capsules formed at high powers, require less amount of tannin per unit and thus with the same amount of tannin that was used for the different studies, more capsules are eventually formed. Another possibility that would explain the just-discussed finding is the well-known concept of a depletion of microstructures by, and in favour of nanostructures; studies to elucidate this effect in case of TMCs are under way.

In the case of the hydrolysable tannin **TA**, the droplets that were formed at both of the powers studied (40 and 160 W), appeared to be much smaller compared to the TMCs obtained in case of the two condensed tannins, and showed in every case mean diameters lower than 1 μm (**Table 2**, entries 5, 6). A comparable behaviour was noticed for the **EGCG** NEs, where the droplets were formed with diameters in the ranges of 0.2 to 2 μm, independently of the acoustic power used (**Table 2**, entries 7, 8).

Table 2 also shows the statistically averaged values of the shell size analysis of three images for each MC sample. In case of the ***Sb*** and ***Am*** tannins, shell dimensions show a significant decrease when high sonication power is applied. When low acoustic power is applied they range from 0.25 to 0.31 μm (**Table 2**, entries 1, 3), whereas an increased power led to smaller shells of 0.13-0.14 μm (**Table 2**, entries 2, 4).The shell in the above cases corresponds to the 14-17% of the whole capsule which represents a thick shell wall, independently of the power used. These findings underline the tuneable character of the method with respect to the shell size that can be easily adjusted to the eventual needs of each application.

In case of the **TA** and **EGCG** tannins, shell thickness is not dependent on different sonication amplitudes. More specifically, shell sizes of 0.12-0.15 nm for the **TA** NEs and 0.17 nm for the

View Article Online
DOI: 10.1039/C7GC02009K

EGCG NEs show a thick shell wall consisting in almost 20% of the droplet surface, both by low or high sonication power treatments.

pH dependent stability of the capsules

Due to their polyphenolic nature, tannins have intriguing pH responsive properties and tannin capsules hence should exhibit pH dependent disassembly characteristics. pH Stability is a particularly important feature of MCs and NEs with respect to the possibility to develop stimuli responsive colloidal systems for targeted release. Coupled with different, eventually tuneable pH-sensitive disassembly profiles, TMCs and TNEs have different potential biomedical applications because of the varying pH in different parts of the body (*e.g.*, blood at pH 7.4, stomach at pH 1.0 to3.0, duodenum at pH 4.8 to 8.2, etc.).[67] A pH stability study was thus carried out varying the pH of the capsule solution. The pH dependent stability of the capsules is reflected on the capsule number and average size as revealed by the optical microscopy analysis (**Figure 9A**). **Figure 9B** and **C** show the number and the mean size of the capsules for comparative analysis as a function of pH.

View Article Online
DOI: 10.1039/C7GC02009K

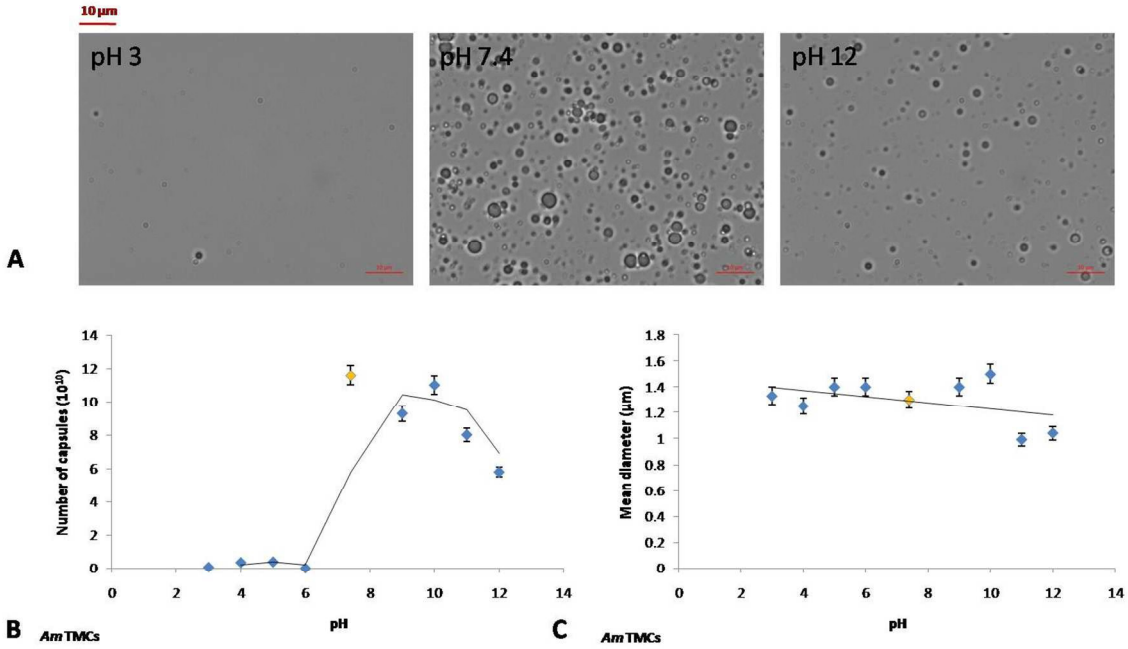

Figure 9: A: Optical microscopy analysis of ***Am*** TMCs subjected to various pH conditions (scale bar 10 µm); B: number of the capsules as function of pH; and C: mean capsule dimensions as function of pH.

0.1 M aqueous MOPS buffer at pH 7.4, which is the standard medium for capsule formation in this study, has proven to be the optimum medium with respect to guarantee stability of once-generated capsules.

Below pH 7, capsules start to disassemble, a phenomenon which is confirmed by both macroscopic and microscopic observation. At pH 3 and 4 the disassembly of the capsules is more pronounced and also macroscopically apparent. These results were confirmed by means of optical microscopy and subsequent size and yield analyses of the systems. As shown in **Figure 9A**and **B**, at pH-values below 6, TMCs are generally unstable. Interestingly, while capsule numbers decreased, the size of the capsules did not significantly change at the different acidic pH values.

At alkaline pH, emulsions are generally more intensely coloured due to elevated degrees of polyphenol deprotonation. Macroscopically, the foamy part consisting in generated capsules was,

View Article Online
DOI: 10.1039/C7GC02009K

however, still evident. The optical microscopy results indicate decreased numbers of droplets; the latter are of significantly smaller sizes (average diameters 1 μm). Deprotonation of the phenolic moieties of tannin occurring under alkaline conditions can probably disassemble the architecture of the bigger aggregates by increasing overall hydrophilicity of the system.

Characterization of Shell-Forming Tannins

GPC analysis

With the aim of clarifying the mechanisms for capsule formation, ***Sb***T and ***Am***T starting materials were submitted to GPC analysis and the results were compared with the GPC analyses of the tannins present in the capsule shells of the respective ***Sb*** and ***Am*** TMCs. In order to remove olive oil residues and avoid as much as possible an oil-tannin overlap, TMCs were destroyed by lyophilizing and residues were extracted with *n*-hexane prior to analysis. It is worth recalling that this procedure ensures that any measured distribution of the molecular weights is relative to the tannin oligomer making up the shell, but not to the capsule unit itself (in case these would be smaller than 450 nm, *i.e.*, the filter size used to prepare samples for GPC analysis). **Figure 10A** and **C** show that ***Sb*** and ***Am*** tannins that formed the shell of capsules obtained at low power of sonication (40 W), have no significant difference in the molecular weight distribution compared to the initial tannins. The same trend was found for the residual tannin that precipitated during the capsule formation, implying that the capsule formation is at low sonication powers is more a result of the unique interactions between aromatic moieties present in the tannins.

View Article Online
DOI: 10.1039/C7GC02009K

It is clear, from **Figure 10B and D**, that the condensed tannins ***Sb*** and ***Am*** constituting the capsules obtained at 160 W, show a significant higher molecular weight distribution than the starting material.[10] On the contrary, the residual tannins recovered after sonication at high powers (160 W) did not show significant differences compared to the starting tannins. Apparently, these findings point towards the occurrence of polymerization reactions due to oxidative coupling induced by ultrasonication during capsules formation at high powers of sonication. However, since the residual tannins were not found polymerized, the hypothesis that the capsules might be formed by a high molecular weight fraction of the starting material, which per chain can undergo more extensive electronic interactions between aromatic moieties during ultrasound treatment appears to be more realistic at this point. Generally, the differences in structures of ***Am*** and ***Sb*** tannins seem to have no impact on the reactivity of the systems during sonication.

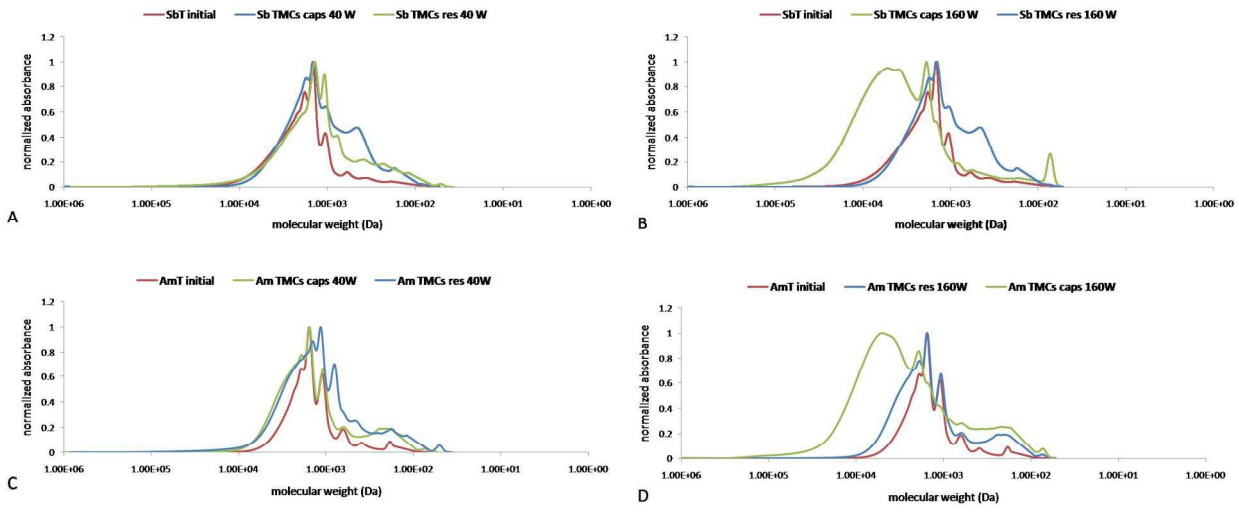

Figure 10: Molecular weight distribution of starting tannins, re-isolated tannins from capsule shells and re-isolated residual tannins after sonication: A: *Schinopsis balansae* tannin (***Sb***T) at 40W; B: ***Sb***T at 160W; C: *Acacia mearnsii* tannin (***Am***T) at 40W; and D: ***Am***T at 160W.

View Article Online
DOI: 10.1039/C7GC02009K

In a similar fashion, NEs obtained from **TA** and **EGCG** were freeze dried, extracted in *n*-hexane and submitted to GPC analysis. In both cases (**Figure 11A** and **B, TA** and **EGCG**, respectively) no significant change was revealed in the distribution of the molecular weight of the tannin in the nanoemulsion and of the starting material, independently from the sonication power used for NE generation. This indicates that cross-linking is actually not extensively occurring under these experimental conditions.

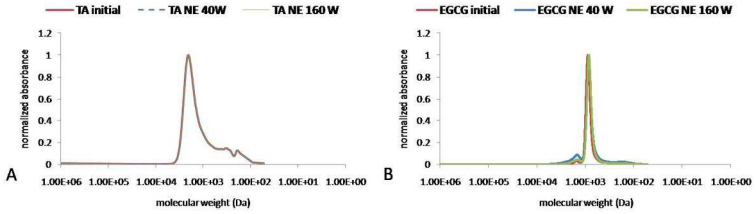

Figure 11: Molecular weight distribution of starting tannins and re-isolated tannins from nanoemulsions synthesized at 40 and 160 W of sonication power, respectively: A: **TA**; B: **EGCG**.

EGCG has the same functional groups as present in ***Am***T. The fact that under sonication **EGCG** does not undergo detectable polymerization further supports the hypothesis that polymerization in general is not likely to occur as a primary process in case of condensed tannins during sonication. If sonication would have generated enough radical species that would undergo extensive oxidative coupling in case of **EGCG**, it would have probably been visible also in case of ***Am***T; in fact, the gallate units present in **EGCG** and **TA** should be in principle even more prone to polymerization than the flavan-3-ol subunits in ***Sb*** and ***Am*** tannins.

One can conclude that the formation of TMCs from ***Sb*** and ***Am*** upon sonication is not, or at least not primarily due to polymerization but to electronic interaction between aromatic moieties of high molecular weight fractions. This also explains why it is not possible to obtain capsules from non-polymeric **TA** and **EGCG**.

View Article Online
DOI: 10.1039/C7GC02009K

The accumulated results also clearly show that the different structures of ***Sb*** and ***Am*** tannins do not have any significant effect on the efficiency of capsule synthesis, their size or behaviour.

Encapsulation Efficiency (EE)

In an effort to assess the encapsulation efficiency (EE) and this the loading capacity of NEs and MCs in view of the development of their possible applications as carriers for active components, a hydrophobic active was first encapsulated in the various capsule systems and was subsequently quantified after the disassembly of the studied systems in organic solvent. The percentual encapsulation efficiency (%EE) of the different colloidal systems was analysed. Coumarin6 was loaded into TMCs and TNEs. The amount of Coumarin 6entrapped was then determined *via* UV-vis spectroscopy against an appropriate calibration curve; the amounts of free Coumarin 6 were detected in the o/w emulsions of TNEs and TMCs after their disassembly in $CHCl_3$. The different EE of the systems were initially calculated as percentages based on the amount of Coumarin 6 that was initially added in the formulation.

SbT and ***Am***T yielded $2.1x10^{11}$ and $9.3x10^{11}$ microcapsules per mL, respectively. (**Table 2**, entries 2 and 4). The ***Sb*** TMCs showed 78% average loading that corresponds to 15.6 µg of encapsulated Coumarin 6 per 0.1 mL of capsules, whereas the 72% of encapsulation in the ***Am*** TMCs corresponds to 14.4 µg of Coumarin 6 per 0.1 mL. The average content of Coumarin 6 was thus found to be 743 ag / ***Sb*** TMC and 155 ag/ ***Am*** TMC, respectively. The ***Am****T* system gave slightly higher microcapsule yields and active loading than the ***Sb****T system*. This could be due to their intrinsic structural diversity. ***Am*** in fact displays phlorglucinolic and pyrogallolic moieties on rings A and B, respectively, while ***Sb*** has a resorcinolic and catecholic oxidative

View Article Online
DOI: 10.1039/C7GC02009K

pattern on the various rings, respectively.[20] The higher amount of phenolic groups per flavan-3-ol unit in ***AmT*** is probably tuning hydrophilicity of the outer shell of the capsules and thus an extension of H-bonding, resulting in overall slightly better performance.

As shown in **Table 2**,the TNEs reveal higher EEs compared to the TMCs. This corresponds to different volumes and numbers of droplets. The absolute value of loading reported in the table is used as representative value for the actual comparison of the systems and is calculated in the following way: in the case of **TA** NE and **EGCG** NE (**Table 2**, entries 6 and 8) the amount of loaded Coumarin 6 (99% and 100%, respectively) is the same as the amount initially dissolved in the oil template during the preparation steps; 20μg and 19.8 μg per mL are efficiently encapsulated in the nanodroplets of **TA** and **EGCG** NEs, respectively. The average loading of Coumarin 6 per droplet can be subsequently normalized based on the yield of the capsules. More specifically, 7.6×10^{11} droplets of the **TA**-NE entrapped 20 μg of Coumarin 6, resulting in average 26 ag per **TA** droplet. Similarly, 6.8×10^{11} **EGCG** microdroplets entrapped 19.8 μg of Coumarin 6, thus in average 29 ag were effectively encapsulated per **EGCG** microdroplet. Most often in literature, the EE is calculated as the ratio of active present inside the carrier to the amount of active that was initially added during the preparation. This value is reported in **Table 2** as %EE.The expression of EE in mass units, *i.e.*, (atto/femto)grams, of active per single droplet or capsule that is calculated based on yield measurements and the encapsulation efficiencies, constitutes an approximation of the encapsulated amount per single entity and is occasionally reported in literature for various delivery systems. Microparticles - with sizes up to 3 or 5 μm- reportedly encapsulate up to some femtograms (fg).[68] In this study, Coumarin 6 was found to be efficiently encapsulated in each single TMC in low amounts of max ~1 fg/capsule. Taking into consideration the smaller diameter of the tannin capsules that were generated in this case (less

View Article Online
DOI: 10.1039/C7GC02009K

than 1 μm diameter) the encapsulation of less material is expected, and the reported TMCs can thus be considered equally efficient systems in the encapsulation of actives compared to various microcapsules found in literature.[68]

To conclude the two systems (TNEs vs TMCs) present a different encapsulation capacity, with the microcapsules having a higher potential in loading active substances, probably due to their more structured shell and free volume for encapsulation. The different encapsulation capacity stems from the different intrinsic nature of capsules and droplets, and from the actual volume and absolute yield of the droplets and capsules that were finally obtained. Overall, MCs represent a more efficient encapsulating system compared to the NEs studied.

Release studies

The release behaviour of TMCs and TNEs was determined by means of UV-vis analysis in phosphate saline buffer (PBS, 0.1 M) at pH 7.4 using TMCs and TNEs loaded with Coumarin 6. The buffer was chosen and prepared in an attempt to simulate the salinity of the human body, in the view of possible biomedical applications of tannin carriers. Aliquots of the released Coumarin 6 from the systems in PBS were collected at specific time intervals and freeze dried for analysis. The dry aliquots were dispersed in 1.0 mL of $CHCl_3$, centrifuged to remove the salts of the buffer and the Coumarin 6 released in the supernatant of each sample was determined *via* UV as a function of time (**Figure 12**).

In all cases, no more than 40% absolute of Coumarin 6 was released in PBS within a 10day-period. This low percentage is due to the extremely low solubility of Coumarin 6 in the aqueous buffer solution, and not to the insufficient destruction of the capsules, which were practically absent by the time the last aliquot was analysed. Many researchers have used Coumarin 6 as a

View Article Online
DOI: 10.1039/C7GC02009K

fluorescent probe of delivery systems in quality and quantity analysis and have come across similar challenges with extremely low cumulative released percentages.[69]

Figure 12 shows the release profiles of Coumarin 6 from TMCs and **TA** and **EGCG** NEs. They are reported as percentages of the releasable Coumarin 6 as a function of time. The profile of Coumarin 6 release from the TMCs shows a burst release after the first 24 hours both for ***Sb***T and ***Am***T, with almost all of the Coumarin 6 eventually released after 10 days.

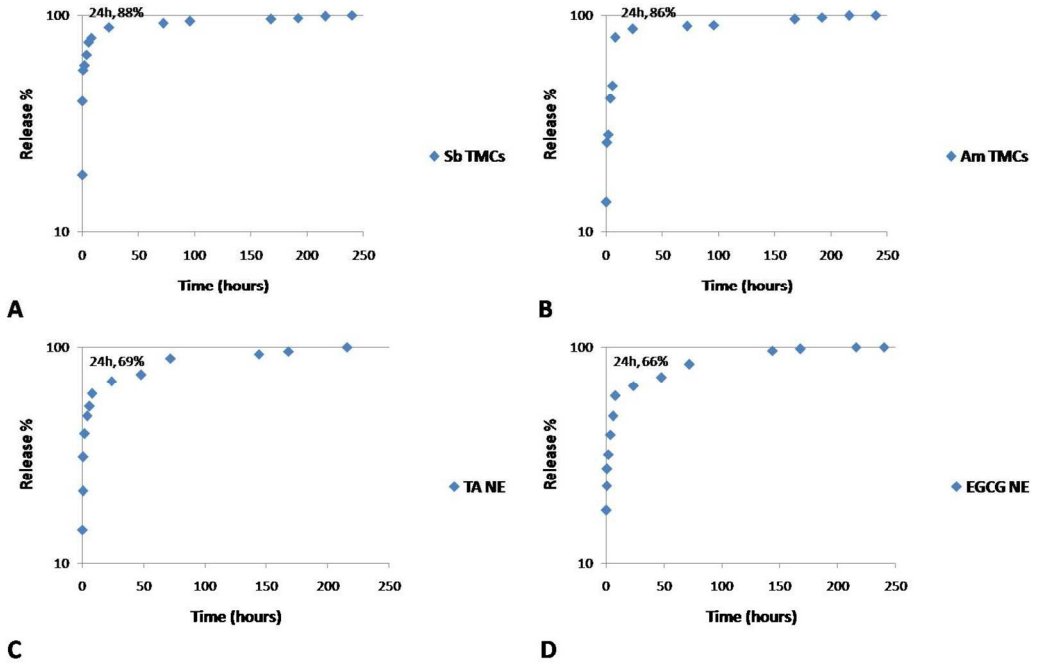

Figure 12: Release profiles of Coumarin 6-filled TMCs and TNEs: A: ***Sb***T; B: ***Am***T; C: **TA**; and D: **EGCG**.

TA and **EGCG** NES show a smoother gradient release profile with respect to MCs from condensed tannins (**Figure 12C**, **D**). NEs can, in general, release extremely high amounts of encapsulated actives. The rate controlling step of the release from TNEs is the corruption of the droplet membrane; after this event, release is characterized by a constant release rate. In the present study, both types of TNEs showed that the destruction of the tannin-based shell is completed after 24 h leading to an afterward steady release.

View Article Online
DOI: 10.1039/C7GC02009K

The present study is the first effort to use **EGCG** as an effective shell for entrapping and delivering actives in a simple and biocompatible formulation, consisting only of the green tea extract and olive oil. **EGCG** was used for the first time in the formation of stable nanoemulsions acting as membrane of the droplet in the stabilization of the nanoemulsion interface for the potential administration of different actives. Thus, based on the results of the encapsulation and release study related to **EGCG**-based TNEs discussed above, **EGCG** can obviously be used as double agent in the formation of delivery microsystems that eventually comprise the two major advantages of the high antioxidant activity and the overall positive health effects associated with the green tea but also of the bioagent that will be additionally incorporated.

Genotoxicity studies

With respect to their use in applications in the fields of functional cosmetics or in the pharmaceutical sector in form of delivery agents, genotoxicity studies were performed on selected samples of only oil-containing MCs and NEs, *i.e.*, ***Am***-based TMCs, ***Sb***-based TMCs and **EGCG**-based TNEs. As genotoxicity-revealing tests were chosen a chromosomal aberration assay, a micronucleus assay and the Comet assay; all tests were performed using Chinese hamster ovary (CHO) cell line, derived from the CHO isolated from an explant of the ovary of a Chinese hamster (*Cricetulusgriseus*, 2n = 22), as originally described by Kao and Puck.[70] The CHO cell line is particularly useful for this kind of studies because of its stable karyotype (modal number is 21 chromosomes), short cell cycle (12–14 h) and its high plating efficiency.

The genotoxic potential of the synthesized TMS was evaluated by analysing the induction of chromosomal aberrations which are highly predictive of long term genetic and cancer risk. Furthermore, due to the specific feature of the assessed material as TMS, the induction of

View Article Online
DOI: 10.1039/C7GC02009K

micronuclei was also evaluated to assess a potential an eugenic effects possibly caused by its interference with the mitotic spindle machinery, while the induction of the primary DNA damage, measured by the use of the alkaline comet assay, was evaluated to more specifically assess a potential generation of reactive oxygen species (ROS) by MCs.

A preliminary dose range finding experiment was performed in order to select the dose levels to be assayed in the main experiments. Potential cytotoxicity and interference with cell cycle progression was assessed by the analysis of the Cytokinesis-Block Proliferation Index (CBPI) for the micronucleus assay while the evaluation of mitotic indices and the frequencies of cells which underwent one (M_1), two (M_2) or more (M_3) replication rounds in the solvent and TMC-treated cells were performed for the chromosomal aberration assay. To discriminate between M_1, M_2 and M_3 cells, DNA was labelled with 5-bromo-2'-deoxyuridine and differential staining of chromatids was obtained using the fluorochrome plus Giemsa staining method. The dose-range finding experiment was performed using a wide range of dose-levels, spaced at 1/4 log intervals, from approximately $2.9x10^9$ to $9.2x10^7$ microcapsules/mL. A severe cytotoxicity was observed at the two highest dose-levels for all the TMC analysed, in which cell proliferation was completely abolished as indicated by the marked reduction of proliferation indices and CBPI. These effects demonstrated that TMC were actually internalized into the cells. At the next lower dose-level of $9.2x10^8$, proliferation indices and CBPI reversed to approximately solvent control levels. This concentration was therefore used for the evaluation of genotoxic effects in the main experiments for all the end-points evaluated.

Results obtained for the induction of chromosomal aberrations, micronuclei and primary DNA damage are collated in **Tables 3-5**, respectively. None of these genotoxic end-points were significantly increased compared to the relevant concurrent solvent control values, indicating that

View Article Online
DOI: 10.1039/C7GC02009K

Am- and ***Sb***-based TMCs and **EGCG**-based TNE, under the reported experimental conditions, do not exhibit any statistically significant genotoxic activity.

Table 3: Analysis of chromosomal aberrations in CHO cells induced by TMCs formed using ***Am*** extracts and ***Sb*** extracts, as well as induced by TNE of **EGCG**.

Compound	Dose level (microcapsules/mL)	Proliferation index	MI (%)[a]	Relative MI[b]	Aberrant cells (%)[c]	Stat. Sig.[d,e]
3 hour treatment						
Solvent	1%	2.01	10,8	100	1.0	-
Am	9.2×10^8	1.88	9.7	90	4.0	NS
Sb	9.2×10^8	1.93	8.9	82	4.0	NS
EGCG	9.2×10^8	1.95	8.0	77	2.0	NS
21 hour treatment						
Solvent	1%	2.01	10.5	100	1.0	-
Am	9.2×10^8	1.92	8.7	83	1.0	NS
Sb	9.2×10^8	1.80	7.8	74	2.0	NS
EGCG	9.2×10^8	1.97	8.3	76	0.0	NS

a: Mitotic indices corresponding to the ratio between the number of cells in a population undergoing mitosis to the number of cells not undergoing mitosis (interphase cells) out of a total of 1000 cells scored and expressed as percentage.
b: Value of MI relative to solvent control considered equal to 100.
c: Aberrant Cells (%): Percentage of cells bearing aberrations (excluding gaps).
d: Statistical significance. To determine the statistical significance of chromosomal aberration induction, the numbers of cells bearing aberrations in the negative control and treated cultures were compared using the Fisher's exact test.
e: Not statistically significant.

View Article Online
DOI: 10.1039/C7GC02009K

Table 4: Analysis of micronuclei in CHO cells induced by the TMCs of ***Am*** and ***Sb*** as well as TNE of **EGCG**.

Compound	Dose level (microcapsules/mL)	CBPI[a]	% Cytostasis[b]	Micronucleated cells (‰)[c]	Stat. Sig.[d,e]
24 hour treatment			-		
Solvent	1%	1.94		4.5	-
Am	9.2×10^8	1.90	4.3	8.0	NS
Sb	9.2×10^8	1.88	6.4	7.0	NS
EGCG	9.2×10^8	1.92	2.1	8.0	NS

a: cytokinesis-block proliferation index.
b: $100 - 100\{(CBPI_T - 1) \div (CBPI_C - 1)\}$ where $CBPI_T$ refers to treated cultures, while $CBPI_C$ refers to solvent control cultures.
c: Incidence of cells bearing 1 or more micronuclei per 1000 cells scored.
d: Statistical significance. To determine the statistical significance of micronucleated cell induction, the numbers of cells bearing micronuclei in the solvent control and treated cultures were compared using the χ^2 test.
e: Not statistically significant.

Table 5: Analysis of DNA breakage by alkaline comet assay induced by TMCs of ***Am***, ***Sb*** and TNE of **EGCG**.

Compound	Dose level (microcapsules/mL)	% Tail Intensity[a]	Stat. Sig.[b,c]
3 hour treatment Solvent	1%	1.59	-
AmT	9.2×10^8	0.35	NS
SbT	9.2×10^8	1.55	NS
EGCG	9.2×10^8	0.98	NS

a: Mean of % tail intensity median values calculated for each slide (50 cells/slide). A total of 150 cells from three independent slides were scored for each experimental point.
b: Statistical significance. To determine the statistical significance of DNA damage induction, the % tail intensity values in the solvent control and treated cultures were compared using the Student's t-test.
c: Not statistically significant.

CONCLUSIONS:

Microstructures based on tannins have been generated for the first time as microdepots to carry and deliver actives other than the inherent ones. Depending on the different structural properties

View Article Online
DOI: 10.1039/C7GC02009K

of the different classes of tannins that were studied, two different colloidal systems were obtained, namely microcapsules (MCs) and nanoemulsions (NEs).The condensed tannins *Schinopsis balansae* (***Sb***) wood extract and *Acacia mearnsii* (***Am***) bark extract assembled upon ultrasonic irradiation into spherical microcapsules of controlled size and architecture with high loading potential for hydrophobic actives like, *e.g.*, Coumarin 6. The hydrolysable tannins tannic acid and epigallocatechin-3-*O*-gallate formed nanoemulsions with the ability to entrap high amounts of bioactive agents.

Both the TMCs and the TNEs generated showed preferably stability at slightly alkaline conditions (pH > 8) and immediate disassembly under acidic conditions (pH < 7). The observed pH stability can be exploited in pH-triggered controlled releases. The two TMC systems and the two TNE systems under study do all show an effective uptake of hydrophobic actives like, e.g., Coumarin 6, and release this active equally well with kinetics and over a timespan that are suitable for considering these systems in pharmaceutical or biomedical applications. This consideration is further justified by the fact that the presented microstructures do not exhibit any statistically relevant genotoxic potential in standard genotoxicity tests.

Overall, the novelty and efficiency of the proposed ultrasound methodology for TMC and TNE generation is an innovative method for the valorisation of tannins. The easy and straightforward method for the formation of tannin based microstructures together with the tuneable character of the process appears extremely promising in the field of development of active delivery vehicles. Moreover, the multifunctionality as well as the complexing properties offered by the tannins themselves gives rise to the concomitant exploitation of various synergistic effects during the development and application of tannin-based MCs and NEs for delivery.

View Article Online
DOI: 10.1039/C7GC02009K

AUTHOR INFORMATION

Corresponding Author

*Email: crestini@stc.uniroma2.it

University of Rome 'Tor Vergata', Department of Chemical Sciences and Technologies, Via dellaRicercaScientifica, 1, 00133 Rome, Italy.

Tel: +39 06 7259 4734

Author Contributions

The manuscript was written through contributions of EDB, HL and CC. The experimental work has been performed by EDB and PM. The interpretation of the results has been done by EDB, HL, PM and CC. All authors have given approval to the final version of the manuscript.

ACKNOWLEDGMENTS

Financial support by the EU-funded research project 'New bio-inspired processes and products from renewable feedstocks – BIO-MIMETIC' (grant agreement No. 282945) is gratefully acknowledged. COST Action FP1306 'Valorisation of lignocellulosic biomass side streams for sustainable production of chemicals, materials & fuels using low environmental impact technologies' and the COST Action FP1105 'Principles of Cell Wall Assembly – Understanding

View Article Online
DOI: 10.1039/C7GC02009K

and Implementation' are acknowledged for providing platforms for discussions. All authors would like to thank Dr Francesca Cavalieri for providing access to the optical microscope and Dr Karsten Thiel for performing the SEM experiments. Luc Zongo, Alessandra Damato and VasileVoloceai are gratefully acknowledged for their contribution in conducting experiments.

ABBREVIATIONS

Am, *Acacia mearnsii* bark extract; ***Am***T, *Acacia mearnsii* tannin; CBPI, cytokinesis-block proliferation index; CHO, Chinese hamster ovary; DMAP, 4-dimethylaminopyridine;DMF, dimethylformamide; DNA, deoxyribonucleic acid; EDTA, ethylenediaminetetraacetic acid; **EGCG**, epigallocatechin-3-*O*-gallate; EE, entrapment efficiency; FITC, fluorescein isothiocyanate; GPC, gel permeation chromatography; HCl, hydrochloric acid; HPLC, high performance liquid chromatography; MC, microcapsule; MOPS, 4- morpholinepropanesulfonic acid; NaOH. Sodium hydroxide; NC, nanocapsule; NE, nanoemulsion; NMR, nuclear magnetic resonance; PBS, phosphate saline buffer; PI, proliferation index; ***Sb***, *Schinopsis balansae* wood extract; ***Sb***T, *Schinopsis balansae* tannin; cryo-SEM, cryogenic scanning electron microscopy; **TA**, tannic acid; THF, tetrahydrofuran; TMC, tannin microcapsule; TNE, tannin nanoemulsion; TMS, tannin microstructure; US, Ultrasound; UV-vis, ultraviolet visible.

View Article Online
DOI: 10.1039/C7GC02009K

REFERENCES

(1) Ochekpe, N. A.; Olorunfemi, P. O.; Ngwuluka, N. C. Nanotechnology and Drug Delivery Part 2: Nanostructures for Drug Delivery. *Tropical Journal of Pharmaceutical Research* **2009**, *8* (3).
(2) Hughes, G. A. Nanostructure-mediated drug delivery. *Nanomedicine* **2005**, *1* (1), 22–30.
(3) Sutradhar, K. B.; Amin, M. L. Nanoemulsions: increasing possibilities in drug delivery. *European Journal of Nanomedicine* **2013**, *5* (2), 97–110.
(4) Freedman, D. *Brownian Motion and Diffusion*; Springer Science & Business Media, 2012.
(5) Jaiswal, M.; Dudhe, R.; Sharma, P. K. Nanoemulsion: an advanced mode of drug delivery system. *3 Biotech* **2015**, *5* (2), 123–127.
(6) Taylor, P. Ostwald ripening in emulsions. *Advances in Colloid and Interface Science* **1998**, *75* (2), 107–163.
(7) Anton, N.; Benoit, J.-P.; Saulnier, P. Design and production of nanoparticles formulated from nano-emulsion templates—A review. *Journal of Controlled Release* **2008**, *128* (3), 185–199.
(8) Mayer, C. Nanocapsules as drug delivery systems. *Int J Artif Organs* **2005**, *28* (11), 1163–1171.
(9) Drozdek, S.; Bazylińska, U. Biocompatible oil core nanocapsules as potential co-carriers of paclitaxel and fluorescent markers: preparation, characterization, and bioimaging. *Colloid Polym Sci* **2016**, *294*, 225–237.
(10) Bartzoka, E. D.; Lange, H.; Thiel, K.; Crestini, C. Coordination Complexes and One-Step Assembly of Lignin for Versatile Nanocapsule Engineering. *ACS Sustainable Chemistry & Engineering* **2016**, *4* (10), 5194–5203.
(11) Tortora, M.; Cavalieri, F.; Mosesso, P.; Ciaffardini, F.; Melone, F.; Crestini, C. Ultrasound Driven Assembly of Lignin into Microcapsules for Storage and Delivery of Hydrophobic Molecules. *Biomacromolecules* **2014**, *15* (5), 1634–1643.
(12) Lin, D.; Liu, N.; Yang, K.; Zhu, L.; Xu, Y.; Xing, B. The effect of ionic strength and pH on the stability of tannic acid-facilitated carbon nanotube suspensions. *Carbon* **2009**, *47* (12), 2875–2882.
(13) Shutava, T.; Prouty, M.; Kommireddy, D.; Lvov, Y. pH Responsive Decomposable Layer-by-Layer Nanofilms and Capsules on the Basis of Tannic Acid. *Macromolecules* **2005**, *38* (7), 2850–2858.
(14) Tian, L.; Pang, Y.; Dixon, R. A. Biosynthesis and genetic engineering of proanthocyanidins and (iso)flavonoids. *Phytochem Rev* **2007**, *7* (3), 445–465.
(15) Khanbabaee, K.; Ree, T. van. Tannins: Classification and Definition. *Nat. Prod. Rep.* **2001**, *18* (6), 641–649.
(16) Riedl, K. M.; Hagerman, A. E. Tannin−Protein Complexes as Radical Scavengers and Radical Sinks. *J. Agric. Food Chem.* **2001**, *49* (10), 4917–4923.
(17) Karamać, M. Chelation of Cu(II), Zn(II), and Fe(II) by Tannin Constituents of Selected Edible Nuts. *International Journal of Molecular Sciences* **2009**, *10* (12), 5485–5497.
(18) Mueller-Harvey, I. Analysis of hydrolysable tannins. *Animal Feed Science and Technology* **2001**, *91* (1–2), 3–20.
(19) Xie, D.-Y.; Dixon, R. A. Proanthocyanidin biosynthesis--still more questions than answers? *Phytochemistry* **2005**, *66* (18), 2127–2144.
(20) Crestini, C.; Lange, H.; Bianchetti, G. Detailed Chemical Composition of Condensed Tannins via Quantitative (31)P NMR and HSQC Analyses: Acacia catechu, Schinopsis balansae, and Acacia mearnsii. *J. Nat. Prod.* **2016**, *79* (9), 2287–2295.
(21) Melone, F.; Saladino, R.; Lange, H.; Crestini, C. Tannin Structural Elucidation and Quantitative 31P NMR Analysis. 1. Model Compounds. *J. Agric. Food Chem.* **2013**, *61* (39), 9307–9315.
(22) Melone, F.; Saladino, R.; Lange, H.; Crestini, C. Tannin Structural Elucidation and Quantitative 31P NMR Analysis. 2. Hydrolyzable Tannins and Proanthocyanidins. *J. Agric. Food Chem.* **2013**, *61* (39), 9316–9324.

View Article Online
DOI: 10.1039/C7GC02009K

(23) Nagle, D. G.; Ferreira, D.; Zhou, Y.-D. Epigallocatechin-3-gallate (EGCG): chemical and biomedical perspectives. *Phytochemistry* **2006**, *67* (17), 1849–1855.
(24) Pizzi, A. Condensed tannins for adhesives. *Ind. Eng. Chem. Prod. Res. Dev.* **1982**, *21* (3), 359–369.
(25) Wheatley, M. J. use of Tannins in Adhesive Applications: Industrial Problems and Potentials. In *Plant Polyphenols*; Hemingway, R. W., Laks, P. E., Eds.; Basic Life Sciences; Springer US, 1992; pp 1005–1011.
(26) Lettinga, G.; Field, J. A.; Sierra-Alvarez, R.; Lier, J. B. van; Rintala, J. Future Perspectives for the Anaerobic Treatment of Forest Industry Wastewaters. *Water Science and Technology* **1991**, *24* (3–4), 91–102.
(27) Sahiner, N.; Sagbas, S.; Sahiner, M.; Silan, C.; Aktas, N.; Turk, M. Biocompatible and biodegradable poly(Tannic Acid) hydrogel with antimicrobial and antioxidant properties. *International Journal of Biological Macromolecules* **2016**, *82*, 150–159.
(28) Alonso-Amelot, M. E.; Oliveros-Bastidas, A.; Calcagno-Pisarelli, M. P. Phenolics and condensed tannins of high altitude Pteridium arachnoideum in relation to sunlight exposure, elevation, and rain regime. *Biochemical Systematics and Ecology* **2007**, *35* (1), 1–10.
(29) Slabbert, N. Complexation of Condensed Tannins with Metal Ions. In *Plant Polyphenols*; Hemingway, R. W., Laks, P. E., Eds.; Basic Life Sciences; Springer US, 1992; pp 421–436.
(30) Ko, C. H.; Lau, K. M.; Choy, W. Y.; Leung, P. C. Effects of tea catechins, epigallocatechin, gallocatechin, and gallocatechin gallate, on bone metabolism. *J. Agric. Food Chem.* **2009**, *57* (16), 7293–7297.
(31) Du, G.-J.; Zhang, Z.; Wen, X.-D.; Yu, C.; Calway, T.; Yuan, C.-S.; Wang, C.-Z. Epigallocatechin Gallate (EGCG) is the most effective cancer chemopreventive polyphenol in green tea. *Nutrients* **2012**, *4* (11), 1679–1691.
(32) Ahmad, N.; Feyes, D. K.; Nieminen, A. L.; Agarwal, R.; Mukhtar, H. Green tea constituent epigallocatechin-3-gallate and induction of apoptosis and cell cycle arrest in human carcinoma cells. *J. Natl. Cancer Inst.* **1997**, *89* (24), 1881–1886.
(33) Higdon, J. V.; Frei, B. Tea catechins and polyphenols: health effects, metabolism, and antioxidant functions. *Crit Rev Food Sci Nutr* **2003**, *43* (1), 89–143.
(34) Bose, M.; Lambert, J. D.; Ju, J.; Reuhl, K. R.; Shapses, S. A.; Yang, C. S. The major green tea polyphenol, (-)-epigallocatechin-3-gallate, inhibits obesity, metabolic syndrome, and fatty liver disease in high-fat-fed mice. *J. Nutr.* **2008**, *138* (9), 1677–1683.
(35) Martinez, C. R.; Iverson, B. L. Rethinking the term “pi-stacking.” *Chem. Sci.* **2012**, *3* (7), 2191–2201.
(36) Hager, A.-S.; Vallons, K. J. R.; Arendt, E. K. Influence of Gallic Acid and Tannic Acid on the Mechanical and Barrier Properties of Wheat Gluten Films. *J. Agric. Food Chem.* **2012**, *60* (24), 6157–6163.
(37) Ru, Q.; Yu, H.; Huang, Q. Encapsulation of Epigallocatechin-3-gallate (EGCG) Using Oil-in-Water (O/W) Submicrometer Emulsions Stabilized by ι-Carrageenan and β-Lactoglobulin. *J. Agric. Food Chem.* **2010**, *58* (19), 10373–10381.
(38) Tsai, Y.-J.; Chen, B.-H. Preparation of catechin extracts and nanoemulsions from green tea leaf waste and their inhibition effect on prostate cancer cell PC-3. *Int J Nanomedicine* **2016**, *11*, 1907–1926.
(39) Lante, A.; Friso, D. Oxidative stability and rheological properties of nanoemulsions with ultrasonic extracted green tea infusion. *Food Research International* **2013**, *54* (1), 269–276.
(40) Wang, Y.-H.; Wan, Z.-L.; Yang, X.-Q.; Wang, J.-M.; Guo, J.; Lin, Y. Colloidal complexation of zein hydrolysate with tannic acid: Constructing peptides-based nanoemulsions for alga oil delivery. *Food Hydrocolloids* **2016**, *54*, *Part A*, 40–48.

View Article Online
DOI: 10.1039/C7GC02009K

(41) Gadkari, P. V.; Balaraman, M. Extraction of catechins from decaffeinated green tea for development of nanoemulsion using palm oil and sunflower oil based lipid carrier systems. *Journal of Food Engineering* **2015**, *147*, 14–23.
(42) Zanchi, D.; Narayanan, T.; Hagenmuller, D.; Baron, A.; Guyot, S.; Cabane, B.; Bouhallab, S. Tannin-assisted aggregation of natively unfolded proteins. *EPL* **2008**, *82* (5), 58001.
(43) Bartzoka, E. D.; Crestini, C.; Lange, H. Biomass Derived and Biomass Inspired Polymers in Pharmaceutical Applications. In *Handbook of Polymers for Pharmaceutical Technologies*; Thakur, V. K., Thakur, nju K., Eds.; John Wiley & Sons, Inc., 2015; pp 127–203.
(44) Manickam, S. *Cavitation : a novel energy-efficient technique for the generation of nanomaterials /*.
(45) Kakran, M.; Antipina, M. N. Emulsion-based techniques for encapsulation in biomedicine, food and personal care. *Current Opinion in Pharmacology* **2014**, *18*, 47–55.
(46) Bartzoka, E. D.; Lange, H.; Crestini, C. Ultrasound-Assisted Functionalization of Polyphenols. In *Handbook of Ultrasonics and Sonochemistry*; Ashokkumar, M., Ed.; Springer Singapore, 2016; pp 1–26.
(47) Ashokkumar, M. The characterization of acoustic cavitation bubbles - An overview. *Ultrasonics sonochemistry* **2010**, *18* (4), 864–872.
(48) Zhou, M.; Cavalieri, F.; Ashokkumar, M. Tailoring the properties of ultrasonically synthesised microbubbles. *Soft Matter* **2011**, *7* (2), 623–630.
(49) Asikkala, J.; Tamminen, T.; Argyropoulos, D. S. Accurate and Reproducible Determination of Lignin Molar Mass by Acetobromination. *J. Agric. Food Chem.* **2012**, *60* (36), 8968–8973.
(50) Lange, H.; Rulli, F.; Crestini, C. Gel Permeation Chromatography in Determining Molecular Weights of Lignins: Critical Aspects Revisited for Improved Utility in the Development of Novel Materials. *ACS Sustain Chem Eng* **2016**, *4* (10), 5167–5180.
(51) Granata, A.; Argyropoulos, D. S. 2-Chloro-4,4,5,5-tetramethyl-1,3,2-dioxaphospholane, a Reagent for the Accurate Determination of the Uncondensed and Condensed Phenolic Moieties in Lignins. *J. Agric. Food Chem.* **1995**, *43* (6), 1538–1544.
(52) Argyropoulos, D. S. 31P NMR in wood chemistry: A review of recent progress. *Res. Chem. Intermed.* **1995**, *21* (3–5), 373–395.
(53) Savage, J. R. Classification and relationships of induced chromosomal structual changes. *J. Med. Genet.* **1976**, *13* (2), 103–122.
(54) Fisher, R. A. On the Interpretation of χ2 from Contingency Tables, and the Calculation of P. *J. R. Stat. Soc.* **1922**, *85* (1), 87–94.
(55) Kirsch-Volders, M.; Sofuni, T.; Aardema, M.; Albertini, S.; Eastmond, D.; Fenech, M.; Ishidate Jr, M.; Kirchner, S.; Lorge, E.; Morita, T. Report from the in vitro micronucleus assay working group. *Mutat. Res. Toxicol. Environ. Mutagen.* **2003**, *540* (2), 153–163.
(56) Yates, F. Contingency table involving small numbers and the χ2 test. *Supplement of J.R. Stat. Soc.* **1934**, *1* (2), 217–235.
(57) Tice, R. R. Single Cell Gel/Comet Assay: Guidelines for in vitro and in vivo Genetic Toxicology Testing. *Environ. Mol. Mutagen.* **2000**, *35* (3), 206–221.
(58) The probable error of a mean student. *Biometrika* **1908**, *6* (1), 1–25.
(59) Sivakumar, M.; Tang, S. Y.; Tan, K. W. Cavitation technology - a greener processing technique for the generation of pharmaceutical nanoemulsions. *Ultrason Sonochem* **2014**, *21* (6), 2069–2083.
(60) Solans, C.; Izquierdo, P.; Nolla, J.; Azemar, N.; Garcia-Celma, M. J. Nano-emulsions. *Current Opinion in Colloid & Interface Science* **2005**, *10* (3–4), 102–110.
(61) Gadkari, P. V.; Balaraman, M. Extraction of catechins from decaffeinated green tea for development of nanoemulsion using palm oil and sunflower oil based lipid carrier systems. *Journal of Food Engineering* **2015**, *147*, 14–23.

View Article Online
DOI: 10.1039/C7GC02009K

(62) Tuyishime, M. A.; Matabaro, E. Green Tea Polyphenols-proteins Nanocomplexes Foaming Behavior, Nanoemulsions and Their Applications. *IJAIR* **2016**, *5* (1), 149–156.
(63) Craig, S.; Beaton, C. D. A simple cryo-SEM method for delicate plant tissues. *Journal of Microscopy* **1996**, *182* (2), 102–105.
(64) Gaumet, M.; Vargas, A.; Gurny, R.; Delie, F. Nanoparticles for drug delivery: The need for precision in reporting particle size parameters. *European Journal of Pharmaceutics and Biopharmaceutics* **2008**, *69* (1), 1–9.
(65) Suslick, K. S.; Didenko, Y.; Fang, M. M.; Hyeon, T.; Kolbeck, K. J.; McNamara, W. B.; Mdleleni, M. M.; Wong, M. Acoustic cavitation and its chemical consequences. *Philosophical Transactions of the Royal Society of London A: Mathematical, Physical and Engineering Sciences* **1999**, *357* (1751), 335–353.
(66) Brotchie, A.; Grieser, F.; Ashokkumar, M. Effect of power and frequency on bubble-size distributions in acoustic cavitation. *Phys. Rev. Lett.* **2009**, *102* (8), 084302.
(67) Schmaljohann, D. Thermo- and pH-responsive polymers in drug delivery. *Advanced Drug Delivery Reviews* **2006**, *58* (15), 1655–1670.
(68) S, J.; G, R.; Aw, T.; Sr, L. Delivery of rapamycin to dendritic cells using degradable microparticles., Delivery of Rapamycin to Dendritic Cells Using Degradable Microparticles. *J Control Release* **2009**, *133*, *133* (3, 3), 191, 191–197.
(69) Gao, H.; Pang, Z.; Fan, L.; Hu, K.; Wu, B.; Jiang, X. Effect of lactoferrin- and transferrin-conjugated polymersomes in brain targeting: in vitro and in vivo evaluations. *Acta Pharmacol. Sin.* **2010**, *31* (2), 237–243.
(70) Kao, F. T.; Puck, T. T. Genetics of somatic mammalian cells, VII. Induction and isolation of nutritional mutants in Chinese hamster cells. *Proc. Natl. Acad. Sci.* **1968**, *60* (4), 1275–1281.

View Article Online
DOI: 10.1039/C7GC02009K

GRAPHICAL ABSTRACT

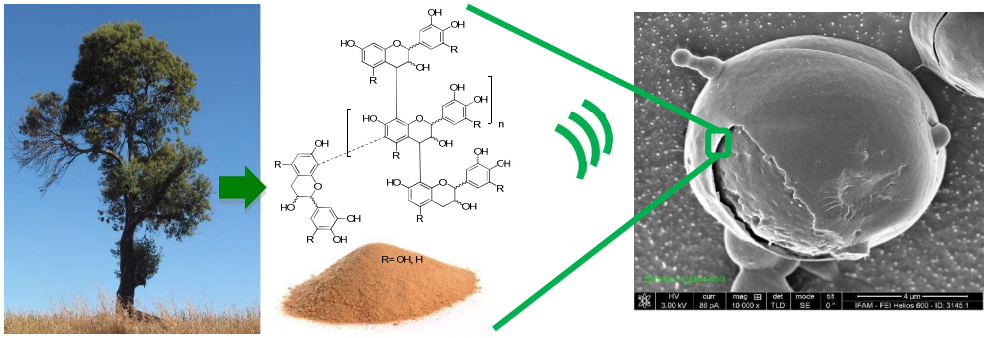

TABLE OF CONTENTS (TOC) GRAPH AND SYNOPSIS

Versatile tannin nano- and microstructures have been created *via* an ultrasound treatment, and thoroughly characterized for the stimuli responsive delivery of active molecules.